C. R. Chimie 13 (2010) 790–802

Contents lists available at ScienceDirect

Comptes Rendus Chimie

www.sciencedirect.com

Full paper/Mémoire

Synthesis, structure, spectroscopy and redox energetics of a series of uranium(IV) mixed-ligand metallocene complexes

Robert K. Thomson, Brian L. Scott, David E. Morris *, Jaqueline L. Kiplinger *

Los Alamos National Laboratory, Los Alamos, NM 87545, USA

ARTICLE INFO

Article history:
Received 2 March 2010
Accepted after revision 1 April 2010
Available online 18 June 2010

Keywords:
Uranium
Amide
Halide
Pseudohalide
Oxidative functionalization
Agostic interactions
η^3-Coordination
Electronic structure
Voltammetry
Mixed-ligand
Metallocenes
UV–visible-near-IR spectroscopy
Weakly-coordinating electrolytes
X-ray crystallography

ABSTRACT

A series of uranium(IV) mixed-ligand amide–halide/pseudohalide complexes $(C_5Me_5)_2U[N(SiMe_3)_2](X)$ (X = F (**1**), Cl (**2**), Br (**3**), I (**4**), N_3 (**5**), NCO (**6**)), $(C_5Me_5)_2U(NPh_2)(X)$ (X = Cl (**7**), N_3 (**8**)), and $(C_5Me_5)_2U[N(Ph)(SiMe_3)](X)$ (X = Cl (**9**), N_3 (**10**)) have been prepared by one electron oxidation of the corresponding uranium(III) amide precursors using either copper halides, silver isocyanate, or triphenylphosphine gold(I)azide. Agostic U···H–C interactions and η^3-(*N,C,C'*) coordination are observed for these complexes in both the solid-state and solution. There is a linear correlation between the chemical shift values of the C_5Me_5 ligand protons in the ^{1}H NMR spectra and the U^{IV}/U^{III} reduction potentials of the $(C_5Me_5)_2U[N(SiMe_3)_2](X)$ complexes, suggesting that there is a common origin, that is overall σ-/π-donation from the ancillary (X) ligand to the metal, contributing to both observables. Optical spectroscopy of the series of complexes **1**–**6** is dominated by the $(C_5Me_5)_2U[N(SiMe_3)_2]$ core, with small variations derived from the identity of the halide/pseudohalide. The considerable π-donating ability of the fluoride ligand is reflected in both the electrochemistry and UV-visible-NIR spectroscopic behavior of the fluoride complex $(C_5Me_5)_2U[N(SiMe_3)_2](F)$ (**1**). The syntheses of the new trivalent uranium amide complex, $(C_5Me_5)_2U[N(Ph)(SiMe_3)](THF)$, and the two new weakly-coordinating electrolytes, $[Pr_4N][B\{3,5\text{-}(CF_3)_2C_6H_3\}_4]$ and $[Pr_4N][B(C_6F_5)_4]$, are also reported.

1. Introduction

Mixed-ligand metallocene complexes of the type $(C_5Me_5)_2U(X)(Y)$ serve as important starting materials for organometallic actinide chemistry, but access to this set of molecules has historically been limited to very specific reaction chemistries [1–7]; consequently, very little is known about the electronic structure and redox energetics for this rare class of compounds. We have been developing oxidative functionalization chemistry of trivalent uranium with copper(I) [8,9] and gold(I) [10] compounds to provide simple and mild methods for synthesizing U^{IV} mixed-ligand metallocene complexes of the type $(C_5Me_5)_2U(X)(Y)$ (where X = halogen, azide, acetylide, etc.; Y = amide). Since uncontrolled oxidation and ligand redistribution are not observed with the Au- or Cu-based $U^{III} \rightarrow U^{IV}$ oxidation procedures, they provide attractive synthetic routes for the preparation of a variety of mixed-ligand metallocene complexes. For example, reaction of the trivalent uranium complex $(C_5Me_5)_2U(NPh_2)(THF)$ with copper(I) iodide or $(Ph_3P)Au\text{-}N_3$ affords the corresponding tetravalent uranium amide-iodide and -azide complexes $(C_5Me_5)_2U(NPh_2)(I)$ [9] and $(C_5Me_5)_2U(NPh_2)(N_3)$ [11], respectively (Eq. (1)).

* Corresponding author.
E-mail addresses: demorris@lanl.gov (D.E. Morris), kiplinger@lanl.gov (J.L. Kiplinger).

1631-0748/$ – see front matter © 2010 Académie des sciences. Published by Elsevier Masson SAS. All rights reserved.
doi:10.1016/j.crci.2010.04.008

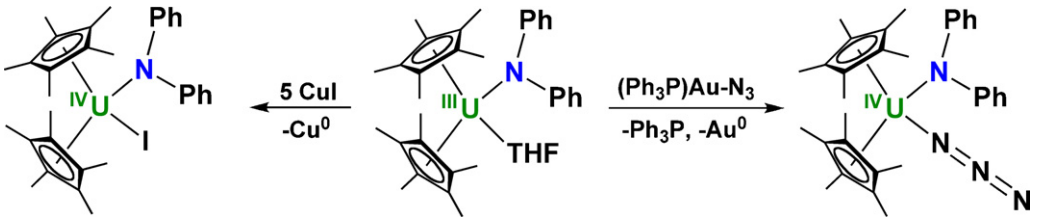

(1)

During the course of these studies, it became evident that the amide mixed-ligand framework provided the opportunity to examine a new homologous structural series from which we can draw new inferences regarding uranium metal–ligand bonding. This falls within the broader context of our continuing efforts to map out trends in the redox energetics and electronic structure of metallocene complexes of the early actinides and correlate these trends with structural chemistry [12–16]. In particular, the amide complexes represent an important end-member along the nitrogenous ligand series: imide (A) [17–20], ketimide (B) [21–24], hydrazonato (C) [2,25–27], amide (D) [8,9,28], as illustrated in Fig. 1.

The uranium–amide bonding interaction should have the lowest degree of π-donation from the nitrogen lone-pair among this series, and this should be reflected in both spectral and electrochemical data. In this contribution, we report the synthesis and structural characterization of a series of mixed-ligand tetravalent uranium complexes of the type $(C_5Me_5)_2U(X)(Y)$ (Y = $N(SiMe_3)_2$, NPh_2, $N(Ph)(SiMe_3)$; X = halide/pseudohalide) from the reaction of Cu, Ag, and Au reagents with the corresponding U^{III} amide precursors. Further, we describe the electrochemical and spectroscopic characterization of a series of related U^{IV} complexes, $(C_5Me_5)_2U[N(SiMe_3)_2](X)$, from this rare class of uranium complexes. We also report the synthesis of the new trivalent uranium amide complex, $(C_5Me_5)_2U[N(Ph)(SiMe_3)](THF)$, and the two new weakly-coordinating electrolytes, $[Pr_4N][B\{3,5\text{-}(CF_3)_2C_6H_3\}_4]$ and $[Pr_4N][B(C_6F_5)_4]$.

2. Results and discussion

2.1. Synthesis and structural characterization

2.1.1. $(C_5Me_5)_2U[N(SiMe_3)_2](X)$ complexes

Oxidative functionalization provides convenient access to mixed-ligand metallocene complexes of the type $(C_5Me_5)_2U(X)(Y)$ (where Y is an amide ligand). As summarized in Scheme 1, reaction of the trivalent uranium amide complex $(C_5Me_5)_2U[N(SiMe_3)_2]$ [29] with various Cu, Ag, and Au reagents afforded the series of related complexes $(C_5Me_5)_2U[N(SiMe_3)_2](X)$ (X = F (**1**), Cl (**2**), Br (**3**), I (**4**), N_3 (**5**), and NCO (**6**)). Specifically, the U^{IV} amide–halide complexes $(C_5Me_5)_2U[N(SiMe_3)_2](F)$ (**1**), $(C_5Me_5)_2U[N(SiMe_3)_2](Cl)$ (**2**), $(C_5Me_5)_2U[N(SiMe_3)_2](Br)$ (**3**), and $(C_5Me_5)_2U[N(SiMe_3)_2](I)$ (**4**) were obtained by oxidation of $(C_5Me_5)_2U[N(SiMe_3)_2]$ using an excess (5 equiv.) of the appropriate Cu halide salt. Separation of the insoluble Cu salts from the reaction products was accomplished by filtration through Celite. Following crystallization, the U^{IV} amide–halide complexes were isolated in moderate to high yields (up to 93%) as crystalline red solids. The amide–azide complex $(C_5Me_5)_2U[N(SiMe_3)_2](N_3)$ (**5**) was prepared in a similar manner using $(Ph_3P)Au\text{-}N_3$ as the oxidant [11]. The complexes were characterized by a combination of ^1H NMR spectroscopy, elemental analyses and X-ray crystallography.

The amide–isocyanate derivative $(C_5Me_5)_2U[N(SiMe_3)_2](NCO)$ (**6**) was synthesized in 71% isolated yield by oxidation of $(C_5Me_5)_2U[N(SiMe_3)_2]$ with AgNCO. Oxidations using copper halides occur over 12 h with an excess of the oxidant (5 equiv.), however use of excess AgNCO or reaction times longer than 2–3 h lead to decomposition of the uranium isocyanate product. This is most likely attributable to the much stronger oxidizing power of Ag^I over Cu^I [30].

The molecular structures of the amide–chloride $(C_5Me_5)_2U[N(SiMe_3)_2](Cl)$ (**2**) (left) and amide–isocyanate $(C_5Me_5)_2U[N(SiMe_3)_2](NCO)$ (**6**) (right) complexes are shown in Fig. 2. Compound **6** represents a rare example of a structurally characterized actinide isocyanate complex, of which there are only two other known complexes [31,32]. Both complexes **2** and **6** feature a bent-metallocene framework with the amide and chloride (for **2**) or isocyanate (for **6**) ligands contained within the metallocene wedge. For $(C_5Me_5)_2U[N(SiMe_3)_2](Cl)$ (**2**), the U(1)–Cl(1) (2.606(3) Å) and U(1)–N(1) (2.268(4) Å) bond lengths are typical of U^{IV}–Cl [3,5,33,34] and U^{IV}–N_{amide} [5,8,9,34–37] bond lengths.

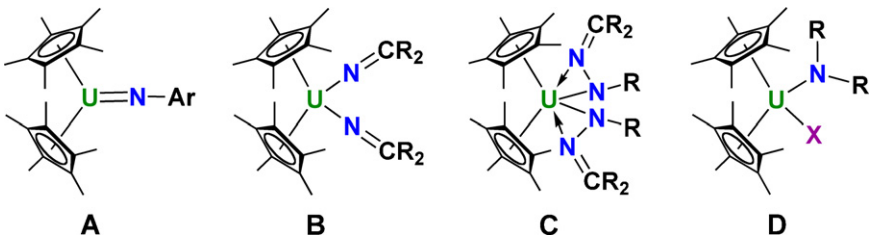

Fig. 1. Uranium metallocene complexes with electronically different nitrogen-based-donor ligands: imide (A), ketimide (B), hydrazonato (C), mixed-amide halide/pseudohalide (D).

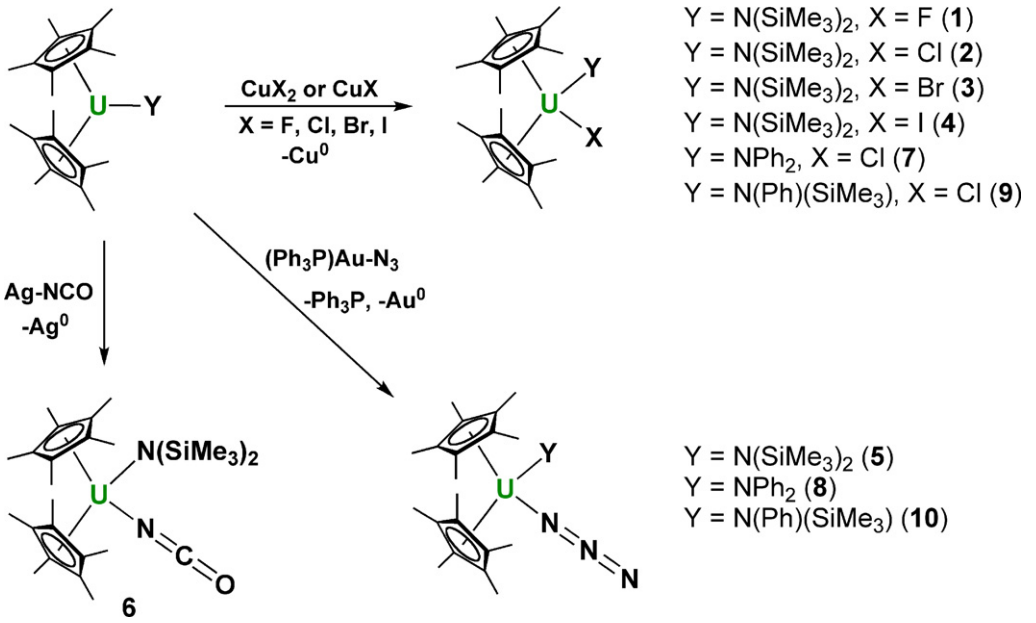

Scheme 1. Mixed-ligand U^{IV} metallocene complexes accessed through oxidative functionalization.

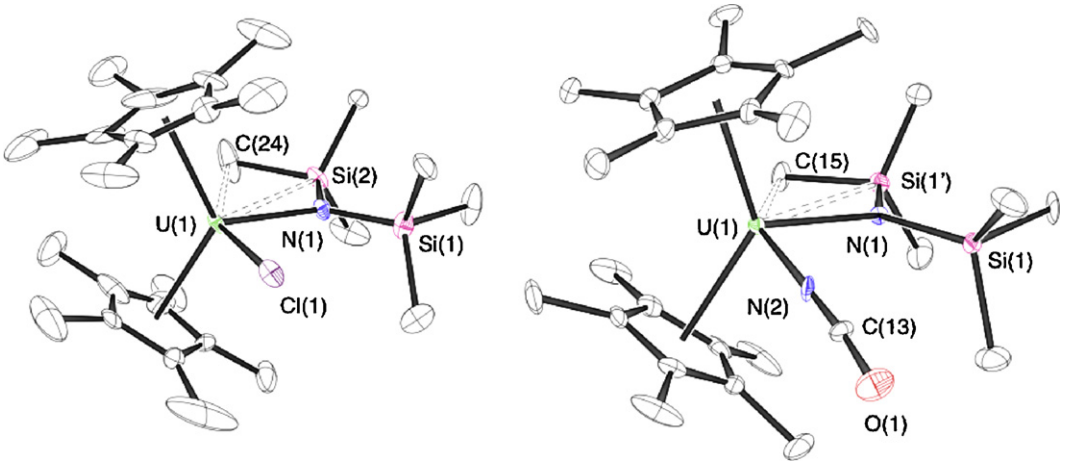

Fig. 2. Molecular structures of $(C_5Me_5)_2U[N(SiMe_3)_2](Cl)$ (**2**) (left) and $(C_5Me_5)_2U[N(SiMe_3)_2](NCO)$ (**6**) (right) with thermal ellipsoids projected at the 30% probability level. Hydrogen atoms have been omitted for clarity. Selected bond lengths (Å) and angles (°) for **2**: U(1)–N(1) 2.268(4), U(1)–Cl(1) 2.606(3), U(1)–C(24) 3.158, U(1)–Si(2) 3.335, Cl(1)–U(1)–N(1) 89.39(14), U(1)–N(1)–Si(1) 130.7(3), U(1)–N(1)–Si(2) 111.2(3), Si(1)–N(1)–Si(2) 118.2(3), U(1)–C(24)–Si(2) 78.2, C(24)–Si(2)–N(1) 107.3(6), N(1)–U(1)–C(24) 63.2. Selected bond lengths (Å) and angles (°) for **6**: U(1)–N(1) 2.241(11), U(1)–N(2) 2.354(16), N(2)–C(13) 1.10(2), C(13)–O(1) 1.29(2), U(1)–C(15) 3.05, U(1)–Si(1′) 3.31, N(1)–U(1)–N(2) 89.2(5), U(1)–N(2)–C(13) 166.4(17), N(2)–C(13)–O(1) 174(3), U(1)–N(1)–Si(1) 128.3(6), U(1)–N(1)–Si(1′) 113.2(6), Si(1)–N(1)–Si(1′) 118.5(6), U(1)–C(15)–Si(1′) 80.7, C(15)–Si(1′)–N(1) 103.9(10), N(1)–U(1)–C(15) 62.0.

For $(C_5Me_5)_2U[N(SiMe_3)_2](NCO)$ (**6**), the isocyanate ligand is bound to the uranium in a linear fashion through the N donor, with a U(1)–N(2) bond distance of 2.354(16) Å, U(1)–N(2)–C(13) bond angle of 166.4(17)°, and N(2)–C(13)–O(1) bond angle of 174(3)°. These metrical parameters compare well with those reported for [(AdArO)$_3$tacn]U(NCO) (U–N = 2.389(6) Å, U–N–C = 171.2(6)°, N–C–O 178.2(9)°)[31] and $[(Me_2N)_3PO]_2UO_2(NCO)_2$ (U–N = 2.336(5) Å, U–N–C = 160.2(5)°, N–C–O = 179.1(7)°) [32]. Additionally, the IR spectrum for complex **6** showed a diagnostic NCO stretch at 2194 cm^{-1}, which is consistent with those observed for the other reported uranium isocyanate complexes (2172–2185 cm^{-1}) [31,32].

A short U–C contact between the methyl group of one of the $SiMe_3$ groups of the $[N(SiMe_3)_2]$ ligand and the uranium center is present in both complexes (**2**: U(1)–C(24) = ~3.14 Å and **6**: U(1)–C(15) = ~3.05 Å). This agostic U···H–C interaction generates a planar U(1)–C(24)–Si(2)–N(1) ring (Σ = 359.8°) in **2** and U(1)–C(15)–Si(1)–N(1) ring (Σ = 359.8°) in **6**. Further support is provided by the different U–N–Si geometric parameters in both complexes **2** and **6**. In $(C_5Me_5)_2U[N(SiMe_3)_2](Cl)$ (**2**), the U(1)–N(1)–

Si(2) angle of 111.2(3)° is significantly smaller than the U(1)–N(1)–Si(1) angle of 130.7(3)°. Similarly, in $(C_5Me_5)_2U[N(SiMe_3)_2](NCO)$ (**6**), the U(1)–N(1)–Si(1′) angle is 113.2(6)° and the U(1)–N(1)–Si(1) angle is 128.3(6)°.

Agostic U···H–C interactions have been previously reported for the structurally related amide-iodide $(C_5Me_5)_2U[N(SiMe_3)_2](I)$ (**4**) [9] and amide–azide $(C_5Me_5)_2U[N(SiMe_3)_2](N_3)$ (**5**) derivatives [11], which have U–C contacts of ~3.28 Å and ~3.23 Å, respectively. Similar interactions have been observed for other uranium complexes bearing the $[N(SiMe_3)_2]$ ligand. Three U···H–C interactions ($U–C_{ave}$ = ~3.31 Å) were proposed to exist in the U^{IV} complex $[(Me_3Si)_2N]_3U–S(2,6\text{-}Me_2C_6H_3)$ [38], while the U^{III} metallocene complex $(C_5Me_5)U[N(SiMe_3)_2]_2$ featured two U···H–C interactions ($U–C_{ave}$ = ~2.83 Å) [39]. Decreased U–N–Si angles were also hallmarks for U···H–C interactions in these complexes.

Interestingly, these solid-state agostic U···H–C interactions are also maintained in solution. For example, the ^{1}H NMR spectrum for $(C_5Me_5)_2U[N(SiMe_3)_2](Cl)$ (**2**) shows three different $SiMe_3$ environments at δ 7.42, 4.31, and −107.98 in a 3:2:1 ratio. The considerably upfield shifted methyl signal at δ −107.98, which integrates to three protons, is consistent with restricted rotation of the $SiMe_3$ group due to the presence of an agostic U···H–C interaction between one of the Si–Me groups and the uranium center. The two methyl groups not involved in the agostic interaction appear as a single resonance at δ 4.31, while the freely rotating $SiMe_3$ group is present at δ 7.42. The C_5Me_5 groups are equivalent and give rise to a singlet at δ 10.29. A similar four signal pattern is observed for the entire series of complexes $(C_5Me_5)_2U[N(SiMe_3)_2](X)$ (X = F (**1**), Cl (**2**), Br (**3**), I (**4**), N_3 (**5**), NCO (**6**)), and these data are summarized in Table 1.

There is a relationship between the chemical shift for like protons (i.e. the C_5Me_5 resonances) and the identity of the ancillary (X) ligand in the paramagnetic $5f^2$ $(C_5Me_5)_2U[N(SiMe_3)_2](X)$ framework. The data in Table 1 show that the chemical shift of the C_5Me_5 group moves upfield with variation of the halide/pseudohalide ligand from I → Br → Cl → NCO → N_3 → F. In effect, the better the π-donor, the more electron-rich the uranium center, which results in a larger shielding and an upfield shift of the auxiliary ligand protons. Similar trends have been observed for other paramagnetic trivalent [40], tetravalent [41,42] and pentavalent [15,16,43,44] uranium systems. Not surprisingly, the data in Table 1 also demonstrate that the chemical shift of the Si–Me group engaged in the agostic U···H–C interaction with the uranium center is sensitive to the nature of the (X) group and moves downfield with variation of the halide/pseudohalide from I ~ Br → Cl → NCO → N_3 → F. Thus, the better the π-donor, the more electron-rich the uranium center, which yields a weaker agostic U···H–C interaction and subsequently a downfield shift of the Si–Me protons. The chemical shift of analogous protons within the $(C_5Me_5)_2U[N(SiMe_3)_2](X)$ series track with the electron density at the U^{IV} center and this is in good agreement with the electrochemical data which suggest a similar trend in ease of reduction across the series (vide infra).

2.1.2. $(C_5Me_5)_2U(NPh_2)(X)$ complexes

Under conditions identical to those employed for the synthesis of $(C_5Me_5)_2U[N(SiMe_3)_2](Cl)$ (**2**) and $(C_5Me_5)_2U[N(SiMe_3)_2](N_3)$ (**5**), the U^{III} complex $(C_5Me_5)_2U(NPh_2)(THF)$ [8] was smoothly oxidized with CuCl and $(Ph_3P)Au\text{-}N_3$ to afford the corresponding U^{IV} amide–chloride $(C_5Me_5)_2U(NPh_2)(Cl)$ (**7**) and U^{IV} amide–azide $(C_5Me_5)_2U(NPh_2)(N_3)$ (**8**) complexes, respectively (Scheme 1). Following workup by filtration through Celite and crystallization, **7** and **8** were reproducibly isolated as analytically pure solids and characterized by a combination of ^{1}H NMR spectroscopy, elemental analyses and X-ray crystallography.

The molecular structure of the amide–chloride complex $(C_5Me_5)_2U(NPh_2)(Cl)$ (**7**) is given in Fig. 3 and reveals the typical bent-metallocene framework with the amide and chloride ligands contained within the metallocene wedge. The structure of $(C_5Me_5)_2U(NPh_2)(Cl)$ (**7**) is similar to that of $(C_5Me_5)_2U[N(SiMe_3)_2](Cl)$ (**2**) and the U–Cl and $U–N_{amide}$ bond distances are comparable. In complex **7**, there is a close U–C contact between the uranium center and one of the *ortho* carbon atoms of one of the phenyl rings of the $[NPh_2]$ ligand (U(1)–C(32) = ~3.41 Å, U(1)–H(32) = ~2.87 Å). This interaction also generates a nearly planar U(1)–N(1)–C(27)–C(32) ring, with the sum of angles being 359.0°.

Unlike the U···H–C interaction which persists in solution for the isostructural iodide complex $(C_5Me_5)_2U(NPh_2)(I)$ [9], the ^{1}H NMR spectrum for $(C_5Me_5)_2U(NPh_2)(Cl)$ (**7**) shows that in solution the NPh_2 ligand is freely rotating and appears as a single broad resonance at δ 15.53 with a sharp singlet at δ 12.73 for the C_5Me_5 protons. In contrast, $(C_5Me_5)_2U(NPh_2)(I)$ has a highly upfield shifted Ar–*H* proton (δ −146.83) relative to the other proton signals [9]. This observation that the U···H–C interaction in $(C_5Me_5)_2U(NPh_2)(Cl)$ (**7**) is weaker than that in $(C_5Me_5)_2U(NPh_2)(I)$ is consistent with the trend noted above for the $(C_5Me_5)_2U[N(SiMe_3)_2](X)$ complexes: the better the π-donor, the more electron-rich the uranium center, which yields a weaker U···H–C interaction. These

Table 1
^{1}H NMR spectroscopic data for $(C_5Me_5)_2U[N(SiMe_3)_2](X)$.

Complex	δ C_5Me_5	δ $SiMe_3$	δ $SiMe_2$	δ SiMe
$(C_5Me_5)_2U[N(SiMe_3)_2](F)$ (**1**)	5.95	−0.78	−0.33	−58.26
$(C_5Me_5)_2U[N(SiMe_3)_2](Cl)$ (**2**)	10.29	7.42	4.31	−107.98
$(C_5Me_5)_2U[N(SiMe_3)_2](Br)$ (**3**)	11.40	8.41	4.51	−109.75
$(C_5Me_5)_2U[N(SiMe_3)_2](I)$ (**4**)	12.84	9.22	4.83	−109.70
$(C_5Me_5)_2U[N(SiMe_3)_2](N_3)$ (**5**)	8.69	4.84	3.33	−102.36
$(C_5Me_5)_2U[N(SiMe_3)_2](NCO)$ (**6**)	8.92	6.12	5.15	−105.78

Spectra collected in C_6D_6 with chemical shifts given in parts per million (ppm) relative to $SiMe_4$ (0.00).

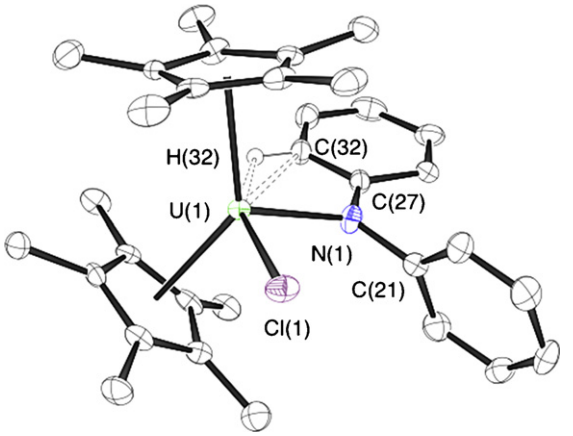

Fig. 3. Molecular structure of $(C_5Me_5)_2U(NPh_2)(Cl)$ (**7**) with thermal ellipsoids projected at the 50% probability level. Hydrogen atoms have been omitted for clarity. Selected bond lengths (Å) and angles (°): U(1)–N(1) 2.286(5), U(1)–Cl(1) 2.6099(15), U(1)–C(32) 3.410, U(1)–H(32) 2.870, Cl(1)–U(1)–N(1) 98.93(13), U(1)–N(1)–C(21) 121.8(4), U(1)–N(1)–C(27) 122.3(4), C(21)–N(1)–C(27) 115.9(5), U(1)–C(32)–C(27) 71.9, C(32)–C(27)–N(1) 119.9(5), C(32)–U(1)–N(1) 44.9.

data also suggest that the U···H–C_{aryl} interaction in $(C_5Me_5)_2U(NPh_2)(Cl)$ (**7**) is weaker than the U···H–C interaction observed for $(C_5Me_5)_2U[N(SiMe_3)_2](Cl)$ (**2**).

Close U–C contacts have been observed previously between uranium and aryl amides. For example, the bridged amide system $\{[(Me_3Si)_2N]_2U(\mu\text{-}NH(2,4,6\text{-}Me_3C_6H_2))\}_2$ exhibits several close U–$C_{mesityl}$ interactions with U–C distances of ~3.10–3.39 Å [45]. A close U–C_{ipso} contact of ~2.94 Å with one of the phenyl rings of the NPh_2 ligand in the hydrotris(3,5-dimethylpyrazolyl)borate uranium complex $[U(Tp^{Me2})Cl_2(NPh_2)]$ has also been reported [35]. This interaction also results in a decrease in the U–N–C_{ipso} angle to 105.5(8)° for the interacting phenyl group versus 140.2(8)° for the non-interacting group [35].

2.1.3. $(C_5Me_5)_2U[N(Ph)(SiMe_3)](X)$ complexes

Given the interesting solid-state and solution agostic U···H–C interactions seen for the $(C_5Me_5)_2U[N(SiMe_3)_2](X)$ and $(C_5Me_5)_2U(NPh_2)(X)$ systems, the new trivalent uranium amide complex, $(C_5Me_5)_2U[N(Ph)(SiMe_3)](THF)$ was prepared to determine which type of U···H–C interaction ($SiMe_3$ or phenyl) would be dominant. As shown in Eq. (2), reaction of $(C_5Me_5)_2U(I)(THF)$ with $(THF)K[N(Ph)(SiMe_3)]$ afforded $(C_5Me_5)_2U[N(Ph)(SiMe_3)](THF)$ as a green crystalline solid in 65% isolated yield.

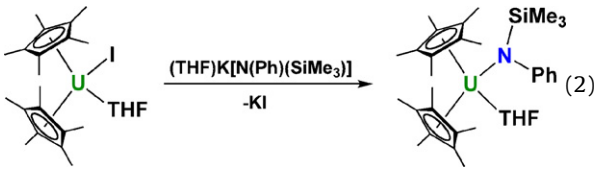

(2)

As with the other U^{III} amide complexes, $(C_5Me_5)_2U[N(Ph)(SiMe_3)](THF)$ is readily oxidized with CuCl and $(Ph_3P)Au\text{-}N_3$ to form the corresponding U^{IV} amide–chloride $(C_5Me_5)_2U[N(Ph)(SiMe_3)](Cl)$ (**9**) and U^{IV} amide–azide $(C_5Me_5)_2U[N(Ph)(SiMe_3)](N_3)$ (**10**) complexes, respectively (Scheme 1). Following workup by filtration through Celite and crystallization, **9** and **10** were reproducibly isolated as analytically pure solids in 80% isolated yield and characterized by a combination of ^1H NMR spectroscopy, elemental analyses and X-ray crystallography.

The molecular structures of $(C_5Me_5)_2U[N(Ph)(SiMe_3)](Cl)$ (**9**) (left) and $(C_5Me_5)_2U[N(Ph)(SiMe_3)](N_3)$ (**10**) (right) are provided in Fig. 4. Both complexes **9** and **10** feature a bent-metallocene framework with the amide and chloride (for **9**) or azide (for **10**) ligands contained within the metallocene wedge. The structure of $(C_5Me_5)_2U[N(Ph)(SiMe_3)](Cl)$ (**9**) is similar to that of $(C_5Me_5)_2U[N(SiMe_3)_2](Cl)$ (**2**) and $(C_5Me_5)_2U(NPh_2)(Cl)$ (**7**), with the U–Cl and U–N_{amide} bond distances being comparable. Likewise, the azide ligand in $(C_5Me_5)_2U[N(Ph)(SiMe_3)](N_3)$ (**10**) is bound in a linear fashion with a U(1)–N(1)–N(2) bond angle of 176.8(6)° and a N(1)–N(2)–N(3) bond angle of 177.9(10)° and is akin to the structurally related and previously characterized azide complexes $(C_5Me_5)_2U[N(SiMe_3)_2](N_3)$ (**5**) [11], $(C_5Me_5)_2U(NPh_2)(N_3)$ (**8**) [11], and $(C_5Me_5)_2U(O\text{-}2,6\text{-}{}^iPr_2C_6H_3)(N_3)$ [10].

The amide ligands in both $(C_5Me_5)_2U[N(Ph)(SiMe_3)](Cl)$ (**9**) and $(C_5Me_5)_2U[N(Ph)(SiMe_3)](N_3)$ (**10**) also exhibit short U–C contacts, but these interactions are considerably different from that of $(C_5Me_5)_2U(NPh_2)(Cl)$ (**7**) in that the rings formed by U(1)–N(1)–C(21)–C(22) ($\Sigma = 343.5°$) for **9** and U(1)–N(4)–C(24)–C(25) ($\Sigma = 345.2°$) for **10** are non-planar. Furthermore, these interactions result in a marked decrease in the U–N–C_{ipso} angle, with U(1)–N(1)–C(21) = 105.32(16)° for **9** and U(1)–N(4)–C(24) = 103.6(5)° for **10** versus U(1)–N(1)–C(27)/C(21) = 122.3(4)/121.8(4)° for **7**.

The $[N(Ph)(SiMe_3)]$ ligand is structurally analogous to a benzyl (CH_2Ph) ligand and is coordinated to the uranium metal center in an η^3-(*N,C,C'*)-fashion in $(C_5Me_5)_2U[N(Ph)(SiMe_3)](Cl)$ (**9**) and $(C_5Me_5)_2U[N(Ph)(SiMe_3)](N_3)$ (**10**). The strongest secondary interaction occurs between the uranium and C_{ipso} of the phenyl ring of the coordinated $[N(Ph)(SiMe_3)]$ ligand (**9**: U–C_{ipso} = ~2.98 Å; **10**: U–C_{ipso} = ~2.94 Å) with a weaker unsymmetrical secondary interaction taking place between the uranium and one of the *ortho* carbons atoms of the phenyl ring of the $[N(Ph)(SiMe_3)]$ ligand (**9**: U–C(22) = ~3.18 Å, U–C(26) = ~4.16 Å; **10**: U–C(25) = ~3.05 Å, U–C(29) = ~4.14 Å).

For benzyl complexes, two parameters have been defined to quantify the benzyl ligand-to-metal interaction, Δ and Δ', where $\Delta = [MC_o - MCH_2] - [MC_{ipso} - MCH_2]$ and $\Delta' = [MC_o' - MCH_2] - [MC_{ipso} - MCH_2]$, where MC_o is the shorter metal-to-C_{ortho} contact, MC_o· is the longer metal-to-C_{ortho} contact, MCH_2 is the metal-to-methylene carbon bond length, and MC_{ipso} is the metal-to-C_{ipso} bond length [22,46–48]. For the f-block metals, Δ and Δ' have been shown to have comparable values for an η^4-benzyl-to-metal bonding interaction [22,48], with larger differences between Δ and Δ' being indicative of an η^3-benzyl-to-metal interaction [47].

By extension to the $[N(Ph)(SiMe_3)]$ ligand, Δ and Δ' can be similarly defined for phenyl amide ligands: $\Delta = [MC_o - MN] - [MC_{ipso} - MN]$ and $\Delta' = [MC_o' - MN] - [MC_{ipso} - MN]$, where MC_o is the shorter metal-to-C_{ortho}

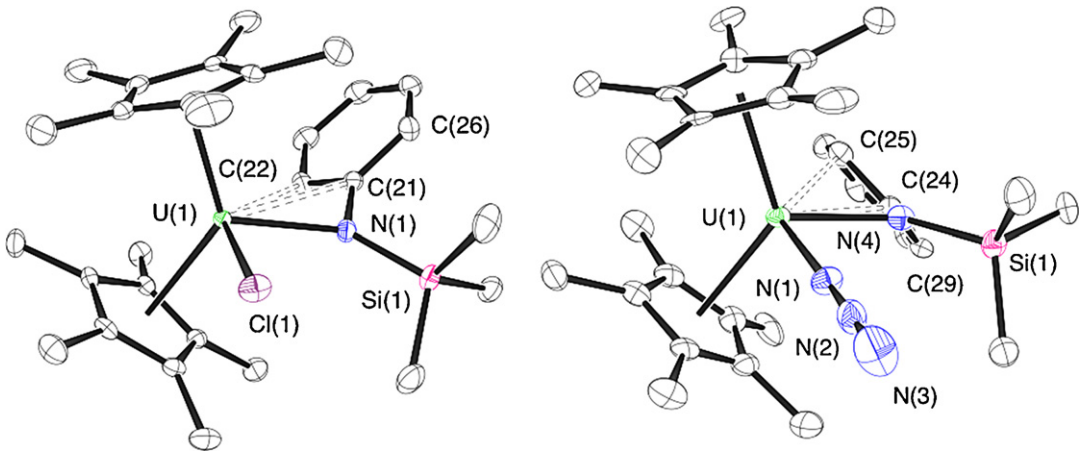

Fig. 4. Molecular structures of $(C_5Me_5)_2U[N(Ph)(SiMe_3)](Cl)$ (**9**) (left) and $(C_5Me_5)_2U[N(Ph)(SiMe_3)](N_3)$ (**10**) (right) with thermal ellipsoids projected at the 50% probability level. Hydrogen atoms have been omitted for clarity. Selected bond lengths (Å) and angles (°) for **9**: U(1)–N(1) 2.275(2), U(1)–Cl(1) 2.5991(7), U(1)–C(22) 3.179, U(1)–C(21) 2.979, U(1)–C(26) 4.155, Cl(1)–U(1)–N(1) 89.12(6), U(1)–N(1)–Si(1) 137.08(12), U(1)–N(1)–C(21) 105.32(16), C(21)–N(1)–Si(1) 117.31(17), U(1)–C(22)–C(21) 68.99, C(22)–U(1)–N(1) 49.54, C(22)–C(21)–N(1) 119.63. Selected bond lengths (Å) and angles (°) for **10**: U(1)–N(1) 2.243(6), U(1)–N(4) 2.268(7), N(1)–N(2) 1.201(9), N(2)–N(3) 1.133(10), U(1)–C(25) 3.053, U(1)–C(24) 2.937, U(1)–C(29) 4.141, N(1)–U(1)–N(4) 85.6(2), U(1)–N(1)–N(2) 176.8(6), N(1)–N(2)–N(3) 177.9(10), U(1)–N(4)–Si(1) 135.5(3), U(1)–N(4)–C(24) 103.6(5), C(24)–N(4)–Si(1) 119.8(5), U(1)–C(25)–C(24) 71.85, C(25)–C(24)–N(4) 118.3(7), C(25)–U(1)–N(4) 51.40.

Table 2
Bond lengths for uranium arene interactions for uranium phenyl amide complexes.

Complex	$MC_{ipso} - MN$[a]	$MC_o - MN$[b]	$MC_o' - MN$[c]	Δ[d]	Δ'[e]
$[U][N(Ph)(SiMe_3)](Cl)$ (**9**)	0.70	0.90	1.88	0.20	1.18
$[U][N(Ph)(SiMe_3)](N_3)$ (**10**)	0.67	0.79	1.87	0.12	1.20
$[U_4(NPh)_6I_4(py)_6]\cdot 5py$	0.48	0.59	1.57	0.11	1.09

[a] Uranium-to-*ipso* carbon bond length minus uranium-nitrogen bond length.
[b] Uranium-to-shorter *ortho* carbon bond length minus uranium-nitrogen bond length.
[c] Uranium-to-longer *ortho* carbon bond length minus uranium-nitrogen bond length.
[d] $[(MC_o - MN) - (MC_{ipso} - MN)]$.
[e] $[(MC_o' - MN) - (MC_{ipso} - MN)]$. $[U] = (C_5Me_5)_2U$.

contact, MC_o' is the longer metal-to-C_{ortho} contact, MN is the metal-to-N_{amide} bond length, and MC_{ipso} is the metal-to-C_{ipso} bond length. Table 2 presents the Δ and Δ' values determined for $(C_5Me_5)_2U[N(Ph)(SiMe_3)](Cl)$ (**9**) and $(C_5Me_5)_2U[N(Ph)(SiMe_3)](N_3)$ (**10**). The metrical parameters exhibited by complexes **9** and **10** (large difference in Δ and Δ' values) support the assignment of η^3-hapticity for the $[N(Ph)(SiMe_3)]$ ligands in these complexes. These compare well with the Δ and Δ' values determined for the other η^3-(*N,C,C'*)-coordinated phenyl imide indentified in the uranium(IV) cluster complex $[U_4(NPh)_6I_4(py)_6]\cdot 5py$ reported by Berthet et al. [49].

The ^1H NMR spectrum for $(C_5Me_5)_2U[N(Ph)(SiMe_3)](Cl)$ (**9**) suggests a rigid structure is maintained in solution as evidenced by two distinct resonances for the *ortho*-aryl protons at δ 8.12 and δ 0.29, and singlets for the C_5Me_5 protons at δ 9.47 and the non-interacting $SiMe_3$ group at δ 5.78, with the *para*-aryl and *meta*-aryl protons appearing at δ 5.90 and δ −10.03, respectively.

The azide complex **10** exhibits a very similar ^1H NMR spectrum, however, the aryl ring does not appear to be as tightly bound as in the chloride derivative **9**. This observation is again consistent with the trends noted above: the better the π-donor (the azide ligand), the more electron-rich the uranium center, which yields a weaker U···H–C interaction, or in this case a weaker U–C contact. For $(C_5Me_5)_2U[N(Ph)(SiMe_3)](N_3)$ (**10**), the resonances for *ortho*-aryl, *para*-aryl, and *meta*-aryl protons appear at δ 0.30, −5.82 and −10.12, respectively. The C_5Me_5 and $SiMe_3$ protons are sharp singlets at δ 8.45 and 1.31, respectively.

2.2. Electrochemical studies

Voltammetric data (cyclic and square wave) were obtained for complexes **1**–**3**, **5**, and **6** in ~0.1 M $[Pr_4N][B\{3,5\text{-}(CF_3)_2C_6H_3\}_4]$/THF solution at a Pt working electrode. Similar studies were also undertaken for the iodide complex (**4**), but the data clearly indicated rapid decomposition of this complex in the solvent/supporting electrolyte solution that precluded extraction of redox potential data. All stable complexes exhibited a reversible U^V/U^{IV} oxidation wave and a reversible U^{IV}/U^{III} reduction wave within the accessible potential range. Half-wave potentials were determined in all cases from the peaks in the square-wave voltammograms, and these values are reported in Table 3 versus the ferrocenium/ferrocene internal standard. Typical cyclic voltammograms obtained at 200 mV/s are illustrated in Fig. 5.

There are two notable points in these data. The first pertains to the electron-donating ability of the ancillary (X) ligand. Previous studies have clearly shown that the redox potentials for the uranium metal-based redox couples in

Table 3
Summary of voltammetric data[a] for $(C_5Me_5)_2U[N(SiMe_3)_2](X)$ complexes in ~0.1 M $[Pr_4N][B\{3,5\text{-}(CF_3)_2C_6H_3\}_4]$/THF solution.

Complex	$E_{1/2}[U^V/U^{IV}]$	$E_{1/2}[U^{IV}/U^{III}]$	$\lvert\Delta E_{1/2}\rvert$[b] (V)
$(C_5Me_5)_2U[N(SiMe_3)_2](F)$ (**1**)	−0.06	−2.35	2.29
$(C_5Me_5)_2U[N(SiMe_3)_2](Cl)$ (**2**)	0.10	−2.04	2.14
$(C_5Me_5)_2U[N(SiMe_3)_2](Br)$ (**3**)	0.12	−1.97	2.09
$(C_5Me_5)_2U[N(SiMe_3)_2](N_3)$ (**5**)	−0.04	−2.15	2.11
$(C_5Me_5)_2U[N(SiMe_3)_2](NCO)$ (**6**)	0.09	−2.06	2.15

[a] $E_{1/2}$ values in volts versus $[(C_5H_5)_2Fe]^{+/0}$.
[b] $|\Delta E_{1/2}| = |E_{1/2}[U^V/U^{IV}] - E_{1/2}[U^{IV}/U^{III}]|$.

bent-metallocene complexes are very sensitive to the electrostatic perturbation induced at the metal by the ancillary ligand(s) [12,15,16,21,22]. In particular, the more strongly electron-donating ancillary ligands destabilize the U^{IV}/U^{III} reduction process, shifting it to more negative potential values. Similarly, the more strongly electron-donating ligands stabilize the U^V oxidation state leading to a concomitant negative shift in the U^V/U^{IV} oxidation wave. In the present study, these redox data suggest that the electrostatic perturbation at the U^{IV} center by the ancillary ligands follows the trend $F \gg N_3 > NCO > Cl > Br$. Based on the relative change in the potential of the U^{IV}/U^{III} couple, the influence of the fluoride ligand is significantly larger than that of the other ancillary ligands, suggesting that the fluoride ion interacts with the metal center in both a σ- and π-donating capacity to amplify its influence on the metal-based redox energetics. The electrostatic influence of these ancillary ligands at the metal center is also reflected in the ^1H NMR spectroscopic chemical shift data described below.

The second observation from these redox data is that the potential separation between the two metal-based U^{IV} couples ($|\Delta E_{1/2}|$, Table 3) is very similar to that seen across a very large range of U^{IV} bent-metallocene complexes reported by us [12]. The average separation for the six complexes investigated here ($|\Delta E_{1/2}|_{ave} = 2.16 \pm 0.03$ V) is nearly identical to that found for the previously reported series of $(C_5Me_5)_2U^{IV}(ketimide)_2$ complexes [21,22]. This implies that the influence of the wedge ligands on the metal-based redox properties is comparable for both reduction and oxidation processes; the U^{III} state is destabilized to the same extent that the U^V state is stabilized.

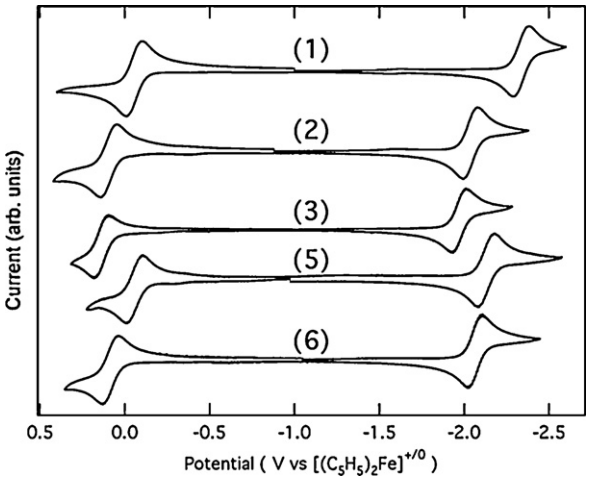

Fig. 5. Cyclic voltammograms obtained at 200 mV/s scan rate for ~2–5 mM solutions of $(C_5Me_5)_2U[N(SiMe_3)_2](X)$ (X = F (**1**), Cl (**2**), Br (**3**), N_3 (**5**), and NCO (**6**)) in ~0.1 M $[Pr_4N][B\{3,5\text{-}(CF_3)_2C_6H_3\}]$/THF at a Pt disk electrode.

The previously observed trend in the chemical shift of the C_5Me_5 protons by ^1H NMR spectroscopy was evaluated through comparison to the electrochemical data collected for complexes **1**–**6**. An excellent linear correlation is observed between the chemical shift of the C_5Me_5 protons and the U^{IV}/U^{III} reduction potential, and is illustrated in Fig. 6. As expected, the $(C_5Me_5)_2U[N(SiMe_3)_2](X)$ complexes bearing weaker electron donors (X = Cl (**2**), Br (**3**), I (**4**)) that gave downfield shifted signals for their C_5Me_5 protons exhibit more positive reduction potentials owing to the greater ease with which they are reduced. The complexes bearing stronger donors (X = N_3 (**5**), NCO (**6**), F (**1**)) are more difficult to reduce and exhibit more negative reduction potentials and more upfield shifted C_5Me_5 proton signals in their ^1H NMR spectra. As illustrated by Fig. 6, the fluoride derivative $(C_5Me_5)_2U[N(SiMe_3)_2](F)$ (**1**) is considerably more electron rich than even the azide (**5**) and isocyanate (**6**) species, suggesting a far greater degree of π-donation from the fluoride anion.

2.3. Spectroscopy

The UV–visible-near IR electronic absorption spectral data for complexes **1**–**6** in toluene solution at room temperature are illustrated in Fig. 7. The data in both the UV–visible region (Fig. 7, top) and the near IR region (Fig. 7, bottom) are similar across this entire series of complexes suggesting that the $(C_5Me_5)_2U[N(SiMe_3)_2]$ structural core provides a highly conserved ligand-field environment that determines the gross features for most of the low-lying electronic transitions. The similarity in the characteristics (moderately intense, rather broad) of the bands found in the visible spectral region for all six complexes, and in particular the very minor influence of the halide ion on these bands, suggests that these are likely charge-transfer (ligand-to-metal and/or metal-to-ligand) transitions as seen in similar U^{IV} bent-metallocene systems [12,21,22,24]. The moderate intensity in these bands, if charge-transfer in character, is consistent with metal f-orbital/ligand orbital parentage in the ground- and excited-states since the intensity scales with orbital overlap and is therefore an indicator of covalency in bonding as described previously [12,21,22,24,50,51].

The consistency in spectral behavior for these six complexes is also found in the NIR spectral region in which

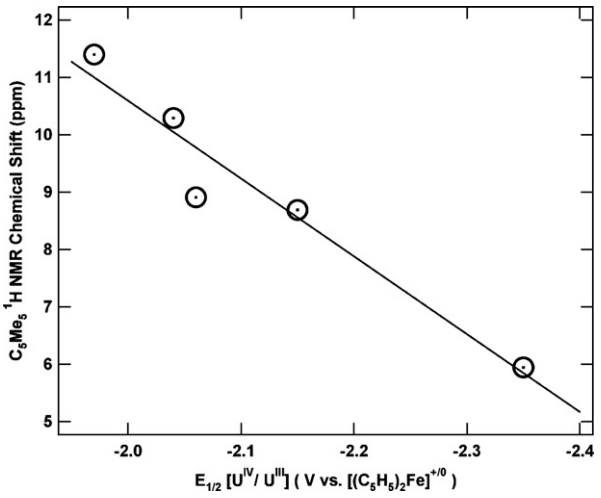

Fig. 6. Linear correlation between ^{1}H NMR chemical shift of C_5Me_5 protons and U^{IV}/U^{III} reduction potential for $(C_5Me_5)_2U[N(SiMe_3)_2](X)$ (X = F (**1**), Cl (**2**), Br (**3**), N_3 (**5**), NCO (**6**)).

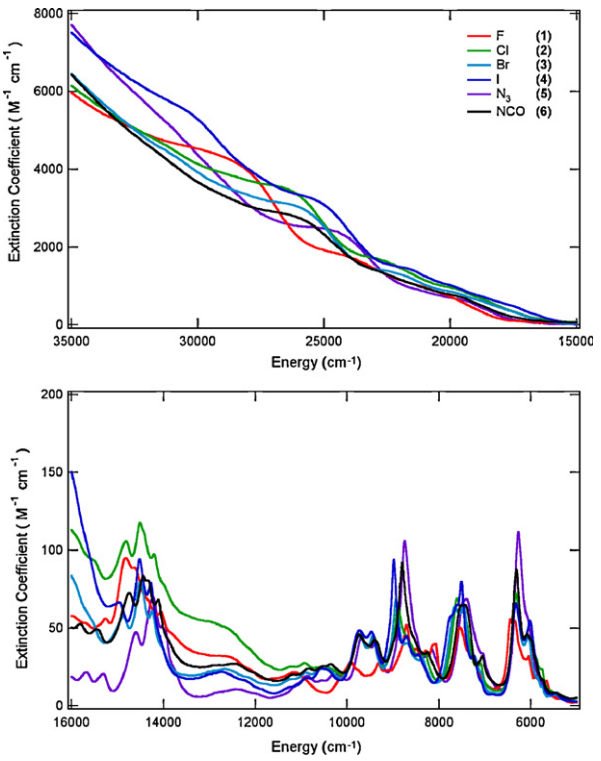

Fig. 7. Electronic absorption spectral data for $(C_5Me_5)_2U[N(SiMe_3)_2](X)$ (X = F (**1**), Cl (**2**), Br (**3**), I (**4**), N_3 (**5**), and NCO (**6**)) in toluene solution at room temperature. Top: UV–visible spectral region. Bottom: near IR spectral region.

the electronic transitions are attributable to states derived from the ground ($^3H_4$) and higher-lying ligand-field manifolds that result from the $5f^2$ valence electronic configuration. The intensity in these bands is on average ~2–3 times less than that found in $(C_5Me_5)_2U^{IV}$(ketimide)$_2$ complexes for which multiple-bond character is observed in the U–N bonds [12,21,22,24]. Thus, consistent with our maturing description of these f–f spectral intensities as markers for metal–ligand covalent bonding, these new spectral data for the $(C_5Me_5)_2U[N(SiMe_3)_2](X)$ complexes indicate that they possess less covalent bonding than found in the U^{IV} ketimides (or U^{IV} and U^{V} imides), but greater than that seen in simple U^{IV} halide or alkyl/aryl complexes [12,15,16,21,22,24,52].

3. Summary

In summary, a series of U^{IV} amide–halide and amide-pseudohalide complexes have been prepared by one-electron oxidations of the corresponding U^{III} amide precursors $(C_5Me_5)_2U[N(SiMe_3)_2]$, $(C_5Me_5)_2U(NPh_2)$, and $(C_5Me_5)_2U[N(Ph)(SiMe_3)]$ using Cu, Ag, and Au salts. Characterization of these complexes in the solid-state revealed close U–C contacts between the ancillary amide ligands and the uranium center that are consistent with agostic U···H–C interactions (for the $(C_5Me_5)_2U[N(SiMe_3)_2](X)$ and $(C_5Me_5)_2U(NPh_2)(X)$ systems) and η^3-(*N,C,C'*)-coordination (for the $(C_5Me_5)_2U[N(Ph)(SiMe_3)](X)$ systems). The series of complexes $(C_5Me_5)_2U[N(SiMe_3)_2](X)$ (X = F (**1**), Cl (**2**), Br (**3**), I (**4**), N_3 (**5**), NCO (**6**)) was examined by electrochemistry and spectroscopy. The reduction potentials for these complexes were directly correlated to the chemical shift values of the C_5Me_5 protons in their ^{1}H NMR spectra. Not only does this make ^{1}H NMR spectroscopy a useful gauge for relative electron density at the uranium center in these complexes, but it also suggests that there is a common origin, namely overall σ- and π-donation from the ancillary (X) ligand to the metal, contributing to both observables. Electronic spectroscopy of these complexes is supportive of the $(C_5Me_5)_2U[N(SiMe_3)_2]$ core dominating the low-lying electronic transitions for these complexes. Transitions between electronic states derived from the $5f^2$ valence electron configuration are considerably weaker than those observed for related U^{IV} ketimide and imide complexes, indicating less covalency for the mixed amide–halide and amide-pseudohalide metallocene complexes presented here, but greater covalency than that observed for simple dihalide or dialkyl/aryl complexes of uranium(IV).

4. Experimental

4.1. General information

Unless otherwise specified, all reactions and manipulations were performed in either a recirculating Vacuum Atmospheres NEXUS model inert atmosphere (N_2) drybox equipped with a 40CFM Dual Purifier NI-Train, or using standard Schlenk techniques. Glassware was dried in an oven at 150 °C overnight prior to use. All NMR spectra were collected using a Bruker Avance 300 MHz NMR spectrometer. Chemical shifts for ^{1}H NMR spectra are reported in parts per million (ppm) and referenced to residual proton solvent impurities calibrated against external TMS. Infrared spectra were collected on a Nicolet Avatar 370 DTGS spectrophotometer. UV-visible-NIR spectra were recorded

using a Perkin-Elmer Lambda 950 spectrophotometer. Mass spectrometric (MS) analyses were performed at the University of California, Berkeley Mass Spectrometry Facility, using a VG Prospec (EI) mass spectrometer. Elemental analyses were performed at either the University of California, Berkeley Microanalytical Facility, on a Perkin-Elmer Series II 2400 CHNS analyzer, Columbia Analytical Services, or Midwest Microlab LLC. Single crystal X-ray diffraction data were collected using a Bruker APEX2 diffractometer. Structural solution and refinement were accomplished using the SHELXL97 suite of software [53–55]. Details regarding data collection are provided in the CIF files.

Except where otherwise noted, reagents were purchased from commercial suppliers and used without further purification. [D_6]Benzene (Aldrich, anhydrous) and [D_8]THF (Cambridge Isotopes, anhydrous) were purified by storage over 4 Å molecular sieves under N_2 prior to use. Celite (Aldrich), alumina (Aldrich, Brockman I), and 4 Å molecular sieves (Aldrich) were dried under dynamic vacuum at 250 °C for 48 h prior to use. All solvents (Aldrich) were purchased anhydrous and dried over KH for 24 h, passed through a column of activated alumina, and stored over activated 4 Å molecular sieves prior to use. The following compounds were prepared according to literature procedures: $(C_5Me_5)_2UI(THF)$ [39], $(C_5Me_5)_2U[N(SiMe_3)_2]$ [29], $(C_5Me_5)_2U(NPh_2)(THF)$ [8], $(Ph_3P)Au\text{-}N_3$ [10], C and [56], and $(C_5Me_5)_2U[N(SiMe_3)_2](I)$ (**4**) [9].

Caution! Depleted uranium (primary isotope ^{238}U) is a weak α-emitter (4.197 MeV) with a half-life of 4.47×10^9 years. Manipulations and reactions should be carried out in monitored fumehoods or in an inert atmosphere drybox in a radiation laboratory equipped with α- and β-counting equipment.

Caution! While we have not observed any explosive behavior with $(Ph_3P)Au\text{-}N_3$ or $(C_5Me_5)_2U[N(SiMe_3)_2](N_3)$ (**5**), all azide complexes are potentially shock sensitive and should be handled with care on an appropriate scale, using personal protection precautions.

4.2. Instrumentation and sample protocols

Electronic absorption spectral data were obtained for toluene solutions of complexes over the wavelength range 300–1600 nm on a Perkin-Elmer Model Lambda 950 UV–visible-near-infrared spectrophotometer. All data were collected in 0.1 cm path length cuvettes loaded in the recirculating Vacuum Atmospheres drybox system discussed above. Samples were typically run at two dilutions, ~0.5 and ~20 mM, to optimize absorbance in the UV–visible and near-infrared, respectively. Spectral resolution was typically 2 nm in the visible region and 4–6 nm in the near-infrared. Sample spectra were obtained versus air and corrected for solvent absorption subsequent to data acquisition.

Cyclic and square wave voltammetric data were obtained in the Vacuum Atmospheres drybox system described above. All data were collected using a Perkin-Elmer Princeton Applied Research Corporation (PARC) Model 263 potentiostat under computer control with PARC Model 270 software. All sample solutions were ~2–3 mM in complex with 0.1 M $[Pr_4N][B\{3,5\text{-}(CF_3)_2C_6H_3\}_4]$ supporting electrolyte in THF solvent. The advantageous properties of quarternary ammonium fluoroarylborate salts like this as electrolytes for voltammetric studies in low dielectric constant solvents have been noted in several recent reports [57,58], and the origin of this advantageous effect has been demonstrated to be directly related to the greater dissociation of the cation/anion pair in low dielectric media such as THF as a result of the more highly delocalized charge in the fluoroaryl borate anions [59]. Furthermore, these anions appear to be more inert towards fluoride abstraction chemistry. We have found that the *n*-propyl ammonium salts are superior to the *n*-butyl ammonium salts by ~2× in reducing solution resistance, with the $[B\{3,5\text{-}(CF_3)_2C_6H_3\}_4]^-$ salt slightly better than the $[B(C_6F_5)_4]^-$ salt in this regard. All data were collected with the positive-feedback IR compensation feature of the software/potentiostat activated to ensure minimal contribution to the voltammetric waves from uncompensated solution resistance (typically ~500 Ω under the conditions employed). Solutions were contained in PARC Model K0264 microcells consisting of a ~3 mm diameter Pt disk working electrode, a Pt wire counter electrode, and a silver wire quasi-reference electrode. Scan rates from 20 to 5000 mV/s were employed in the cyclic voltammetry scans to assess the chemical and electrochemical reversibility of the observed redox transformations. Half-wave potentials were determined from the peak values in the square-wave voltammograms or from the average of the cathodic and anodic peak potentials in the reversible cyclic voltammograms. Potential calibrations were performed at the end of each data collection cycle using the ferrocenium/ferrocene couple as an internal standard. Electronic absorption and cyclic voltammetric data were analyzed using Wavemetrics IGOR Pro (Version 4.0) software on a Macintosh platform.

4.3. Synthesis of $[Pr_4N][B\{3,5\text{-}(CF_3)_2C_6H_3\}_4]$

In a fumehood, a 500-mL Erlenmeyer flask was charged with $Na[B\{3,5\text{-}(CF_3)_2C_6H_3\}_4]$ (8.6 g, 9.7 mmol) and methanol (100 mL), giving an auburn colored solution. A colorless solution of $[Pr_4N][Br]$ (3.1 g, 11.8 mmol) in methanol (100 mL) was added with stirring. The resulting pale yellow solution was stirred at room temperature for 22 h, after which time deionized water (150 mL) was added to the reaction mixture. This immediately generates a thick white precipitate and the reaction becomes warm to the touch. The resulting warm suspension was stirred at room temperature for 10 min and the white solid was collected by filtration using a coarse-porosity fritted filter and washed with deionized water (4 × 150 mL). Each time, the vacuum was disconnected, water added, and the solid was mixed/mashed using a spatula, and then the vacuum reapplied to remove the water. The resulting sticky white solid was then transferred to a 125-mL side-arm flask and dried under vacuum for 24 h. The crude reaction product was taken up into CH_2Cl_2 (40 mL) and the resulting amber colored solution was filtered through a Celite-padded coarse-porosity fritted filter to remove particulates. The filtrate was collected and transferred to a 125-mL

Erlenmeyer flask and layered with diethyl ether (40 mL) followed by hexanes (60 mL). The flask was capped with watch glass and the mixture was allowed to slowly evaporate for 2 days at room temperature during which time the product crystallized from solution. The supernatant was decanted and the solid was washed with hexanes (2 × 50 mL) and air-dried to give **[Pr_4N][B{3,5-(CF_3)$_2$$C_6H_3$}$_4$]** as an off-white crystalline solid (8.6 g, 8.2 mmol, 84%). *Note*: Drying under reduced pressure for 24 h removes coordinated water. ^{1}H NMR ($CDCl_3$, 25 °C, 300 MHz): δ 7.69 (br s, 8 H, Ar-*H*), 7.54 (br s, 4 H, Ar-*H*), 2.93 (m, 8 H, N-CH_2), 1.60 (m, 8 H, CH_2-CH_2-CH_3), 0.94 (t, 12 H, CH_3). ^{19}F NMR ($CDCl_3$, 25 °C, 282 MHz): δ −62.81 (s, 24F, CF_3). Anal. Calcd for $C_{44}H_{40}BF_{24}N{\cdot}2(H_2O)$ (molecular weight 1085.6 g mol^{-1}): C, 48.68; H, 4.09; N, 1.29. Found: C, 48.85; H, 3.83; N, 1.16.

4.4. Synthesis of [Pr_4N][B(C_6F_5)$_4$]

In a fumehood, a 500-mL Erlenmeyer flask was charged with Li[B(C_6F_5)$_4$]·2.5(Et_2O) (7.7 g, 8.8 mmol) and deionized water (100 mL), giving a pale yellow solution. A colorless solution of [Pr_4N][Br] (2.9 g, 11 mmol) in methanol (150 mL) was added with stirring, immediately producing a thick white precipitate. The resulting suspension was stirred at room temperature for 4 h and the white solid was collected by filtration using a coarse-porosity fritted filter and washed with deionized water (5 × 150 mL). Each time, the vacuum was disconnected, water added, and the solid was mixed/mashed using a spatula, and then the vacuum reapplied to remove the water. The resulting sticky white solid was then transferred to a 125-mL side-arm flask and dried under vacuum for 24 h. The crude reaction product was taken up into CH_2Cl_2 (40 mL) and the resulting pale yellow solution was filtered through a Celite-padded coarse-porosity fritted filter to remove particulates. The filtrate was collected and transferred to a 250-mL Erlenmeyer flask and layered with diethyl ether (40 mL) followed by hexanes (60 mL). The flask was capped with a watch glass and the mixture was allowed to evaporate for 2 days at room temperature during which time the product crystallized from solution. The supernatant was decanted and the solid was washed with hexanes (2 × 50 mL) and dried under reduced pressure for 24 h to give **[Pr_4N][B(C_6F_5)$_4$]** as a white crystalline solid (6.7 g, 7.7 mmol, 88%). ^{1}H NMR ($CDCl_3$, 25 °C, 300 MHz): δ 2.99 (m, 8 H, N-CH_2), 1.63 (m, 8 H, CH_2-CH_2-CH_3), 1.01 (t, 12 H, CH_3). ^{19}F NMR ($CDCl_3$, 25 °C, 282 MHz): δ −133.02 (br s, 8 F, *o*-F), −163.20 (t, 4 F, *p*-F), −167.16 (m, 8 F, *m*-F). Anal. Calcd for $C_{36}H_{28}BF_{20}N$ (mol. wt. 865.4 gmol^{-1}): C, 49.96; H, 3.26; N, 1.62. Found: C, 49.95; H, 3.27; N, 1.61.

4.5. Synthesis of (THF)K[N(Ph)($SiMe_3$)]

A 125-mL side-arm flask equipped with a magnetic stir bar was charged with HN(Ph)($SiMe_3$) (5.00 g, 30.2 mmol) and hexanes (50 mL). To this stirred clear solution, K[N($SiMe_3$)$_2$] (6.03 g, 30.2 mmol) was added as a solid at room temperature, giving a white suspension. Approximately 10 mL of THF was added to the suspension to aid in the dissolution of K[N($SiMe_3$)$_2$]. The cloudy white reaction mixture was stirred at room temperature. After 18 h, the reaction mixture was filtered through a medium-porosity fritted filter. The white solid collected was then dried under reduced pressure for 5 h to give **(THF)K[N(Ph)($SiMe_3$)]** (7.03 g, 25.5 mmol, 84%). ^{1}H NMR ([D_8]THF, 25 °C, 300 MHz): δ 6.98 (m, 2 H, *m*-Ar), 6.63-6.50 (m, 3 H, *o*-Ar and *p*-Ar), 3.57 (br, 4 H, O(CH_2CH_2)$_2$), 1.72 (br, 4 H, O(CH_2CH_2)$_2$), 0.22 (s, 6 H, SiMe_2), 0.06 (s, 3 H, Si*Me*).

4.6. Synthesis of (C_5Me_5)$_2$U[N(Ph)($SiMe_3$)](THF)

A 125-mL side-arm flask equipped with a magnetic stir bar was charged with (C_5Me_5)$_2$UI(THF) (0.250 g, 0.353 mmol), toluene (35 mL), and THF (10 mL). To this stirred green solution was added (THF)K[N(Ph)($SiMe_3$)] (0.097 g, 0.353 mmol) as a solid, and the resulting cloudy green–grey solution was stirred at room temperature. After 18 h, the green–brown solution was filtered through a Celite-padded coarse-porosity fritted filter, and the volatiles were removed under reduced pressure. The green-brown residue was extracted into hexane and filtered through a Celite-padded coarse-porosity fritted filter, and the volatiles were removed from the dark green filtrate under reduced pressure to give **(C_5Me_5)$_2$U[N(Ph)($SiMe_3$)](THF)** as a dark green solid (0.170 g, 0.229 mmol, 65%). ^{1}H NMR ([D_6]benzene, 25 °C, 300 MHz): δ 8.12 (s, 1 H, Ar), 3.59 (s, 4 H, O(CH_2CH_2)$_2$), −4.31 (t, J = 7 Hz, 1 H, *p*-Ar), −7.65 (s, 30 H, C_5Me_5), −10.84 (d, J = 5 Hz, 2 H, *o*-Ar), −21.79 (s, 9 H, SiMe_3), −46.30 (br, 1 H, Ar). Satisfactory elemental analysis results could not be obtained due to the thermally sensitive nature of this material.

4.7. Synthesis of (C_5Me_5)$_2$U[N($SiMe_3$)$_2$](Cl) (2)

A 125-mL side-arm flask equipped with a magnetic stir bar was charged with (C_5Me_5)$_2$U[N($SiMe_3$)$_2$] (0.293 g, 0.438 mmol) and toluene (50 mL). To this stirred green-grey solution was added CuCl (0.217 g, 2.19 mmol) as a solid, resulting in an immediate color change to dark red. The resulting solution was stirred at room temperature. After 15 h, the reaction mixture was filtered through a Celite-padded coarse-porosity fritted filter, and the Celite plug was washed with toluene until the washings went colorless. The filtrate was collected and the volatiles were removed under reduced pressure. The resulting red solid was extracted into hexanes and filtered through a Celite-padded coarse-porosity fritted filter, and the Celite plug was washed with hexanes until the washings went colorless. The red colored filtrate was collected and the volatiles were removed under reduced pressure to give **2** as dark red crystals (0.239 g, 0.339 mmol, 77%). ^{1}H NMR ([D_6]benzene, 25 °C, 300 MHz): δ 10.29 (s, 30 H, C_5Me_5), 7.42 (s, 9 H, SiMe_3), 4.31 (s, 6 H, SiMe_2), −107.98 (s, 3 H, Si*Me*). Anal. Calcd for $C_{26}H_{48}ClNSi_2U$ (mol. wt. 704.32 g mol^{-1}): C, 44.34; H, 6.87; N, 1.99. Found: C, 44.07; H, 6.68; N, 1.77.

4.8. Synthesis of (C_5Me_5)$_2$U[N($SiMe_3$)$_2$](Br) (3)

A 125-mL side-arm flask equipped with a magnetic stir bar was charged with (C_5Me_5)$_2$U[N($SiMe_3$)$_2$] (0.250 g,

0.374 mmol) and toluene (50 mL). To this stirred green–grey solution was added CuBr (0.268 g, 1.87 mmol) as a solid, resulting in an immediate color change to dark red. The resulting solution was stirred at room temperature. After 15 h, the reaction mixture was filtered through a Celite-padded coarse-porosity fritted filter, and the Celite plug was washed with toluene until the washings went colorless. The filtrate was collected and the volatiles were removed under reduced pressure. The resulting red solid was extracted into hexanes and filtered through a Celite-padded coarse-porosity fritted filter, and the Celite plug was washed with hexanes until the washings went colorless. The red colored filtrate was collected and the volatiles were removed under reduced pressure to give **3** as a dark red solid (0.145 g, 0.194 mmol, 52%). ^{1}H NMR ([D$_6$]benzene, 25 °C, 300 MHz): δ 11.40 (s, 30 H, C$_5$*Me*$_5$), 8.41 (s, 9 H, Si*Me*$_3$), 4.51 (s, 6 H, Si*Me*$_2$), -109.75 (s, 3 H, Si*Me*). Anal. Calcd for $C_{26}H_{48}BrNSi_2U$ (0.5-C_6H_{14}) (mol. wt. 748.77 g mol^{-1}): C, 43.99; H, 7.00; N, 1.77. Found: C, 44.38; H, 6.68; N, 1.95.

4.9. Synthesis of $(C_5Me_5)_2U[N(SiMe_3)_2](NCO)$ (6)

A 125-mL side-arm flask equipped with a magnetic stir bar was charged with $(C_5Me_5)_2U[N(SiMe_3)_2]$ (0.250 g, 0.374 mmol) and toluene (50 mL). To this stirred green-grey solution was added AgNCO (0.067 g, 0.449 mmol) as a solid, resulting in a color change to dark red. The resulting solution was stirred at room temperature. After 2 h, the reaction mixture was filtered through a Celite-padded coarse-porosity fritted filter, and the Celite plug was washed with toluene until the washings went colorless. The filtrate was collected and the volatiles were removed under reduced pressure. The resulting red solid was extracted into hexanes and filtered through a Celite-padded coarse-porosity fritted filter, and the Celite plug was washed with hexanes until the washings went colorless. The red colored filtrate was collected and the volatiles were removed under reduced pressure to give **6** as dark red crystals (0.190 g, 0.267 mmol, 71%). ^{1}H NMR ([D$_6$]benzene, 25 °C, 300 MHz): δ 8.91 (s, 30 H, C$_5$*Me*$_5$), 6.09 (s, 9 H, Si*Me*$_3$), 5.15 (s, 6 H, Si*Me*$_2$), −105.09 (s, 3 H, Si*Me*). IR (Nujol, cm^{-1}): ν 2194 (s) (NCO asymmetric stretch). Anal. Calcd for $C_{27}H_{48}N_2OSi_2U$ (0.5-C_6H_{14}) (mol. wt. 710.88 g mol^{-1}): C, 47.79; H, 7.35; N, 3.72. Found: C, 47.66; H, 7.01; N, 3.20.

4.10. Synthesis of $(C_5Me_5)_2U(NPh_2)(Cl)$ (7)

A 125-mL side-arm flask equipped with a magnetic stir bar was charged with $(C_5Me_5)_2U(NPh_2)$(THF) (0.537 g, 0.717 mmol) and toluene (50 mL). To this stirred green solution was added CuCl (0.355 g, 3.59 mmol) as a solid, resulting in an immediate color change to dark red. The resulting solution was stirred at room temperature. After 15 h, the reaction mixture was filtered through a Celite-padded coarse-porosity fritted filter, and the Celite plug was washed with toluene until the washings went colorless. The filtrate was collected and the volatiles were removed under reduced pressure. The resulting red solid was extracted into hexanes and filtered through a Celite-padded coarse-porosity fritted filter, and the Celite plug was washed with hexanes until the washings went colorless. The red colored filtrate was collected and the volatiles were removed under reduced pressure to give **7** as a dark red solid (0.440 g, 0.617 mmol, 86%). ^{1}H NMR ([D$_6$]benzene, 25 °C, 300 MHz): δ 15.53 (br, 10 H, Ar), 12.73 (s, 30 H, C$_5$*Me*$_5$). Satisfactory elemental analysis results could not be obtained for this compound despite several attempts. This is most likely due to thermal instability during analysis.

4.11. Synthesis of $(C_5Me_5)_2U[N(Ph)(SiMe_3)](Cl)$ (9)

A 125-mL side-arm flask equipped with a magnetic stir bar was charged with $(C_5Me_5)_2U[N(Ph)(SiMe_3)]$(THF) (0.328 g, 0.440 mmol) and toluene (50 mL). To this stirred green solution was added CuCl (0.131 g, 1.32 mmol) as a solid, resulting in an immediate color change to dark red. The resulting solution was stirred at room temperature. After 15 h, the reaction mixture was filtered through a Celite-padded coarse-porosity fritted filter, and the Celite plug was washed with toluene until the washings went colorless. The filtrate was collected and the volatiles were removed under reduced pressure. The resulting red solid was extracted into hexanes and filtered through a Celite-padded coarse-porosity fritted filter, and the Celite plug was washed with hexanes until the washings went colorless. The red colored filtrate was collected and the volatiles were removed under reduced pressure to give **9** as a dark red solid (0.250 g, 0.353 mmol, 80%). ^{1}H NMR ([D$_6$]benzene, 25 °C, 300 MHz): δ 9.47 (s, 30 H, C$_5$*Me*$_5$), 8.12 (s, 1 H, *o*-Ar), 5.78 (s, 9 H, Si*Me*$_3$), 0.29 (d, J = 5 Hz, 1 H, *o*-Ar), −5.90 (t, J = 7 Hz, 1 H, *p*-Ar), −10.03 (s, 2 H, *m*-Ar). Anal. Calcd for $C_{29}H_{44}ClNSiU$ (mol. wt. 708.23 g mol^{-1}): C, 49.18; H, 6.26; N, 1.98. Found: C, 48.94; H, 5.99; N, 1.62.

4.12. Synthesis of $(C_5Me_5)_2U[N(Ph)(SiMe_3)](N_3)$ (10)

A 125-mL side-arm flask equipped with a magnetic stir bar was charged with $(C_5Me_5)_2U[N(Ph)(SiMe_3)]$(THF) (0.280 g, 0.376 mmol) and toluene (50 mL). To this stirred green solution was added $(Ph_3P)AuN_3$ (0.181 g, 0.376 mmol) as a solid, resulting in an immediate color change to dark red. The resulting solution was stirred at room temperature. After 15 h, the reaction mixture was filtered through a Celite-padded coarse-porosity fritted filter, and the Celite plug was washed with toluene until the washings went colorless. The filtrate was collected and the volatiles were removed under reduced pressure. The resulting red solid was extracted into hexanes and filtered through a Celite-padded coarse-porosity fritted filter, and the Celite plug was washed with hexanes until the washings went colorless. The red colored filtrate was collected and the volatiles were removed under reduced pressure to give **10** as a dark red solid (0.215 g, 0.301 mmol, 80%). ^{1}H NMR ([D$_6$]benzene, 25 °C, 300 MHz): δ 8.45 (s, 30 H, C$_5$*Me*$_5$), 1.31 (s, 9 H, Si*Me*$_3$), 0.30 (s, 2 H, *o*/*m*-Ar), −5.82 (t, J = 7 Hz, 1 H, *p*-Ar), −10.12 (s, 2 H, *o*/*m*-Ar). IR (Nujol, cm^{-1}): ν 2087 (s) (N_3 asymmetric stretch). Anal. Calcd for $C_{29}H_{44}N_4SiU$ (0.5-C_7H_8) (mol. wt. 714.80 g mol^{-1}): C, 51.30; H, 6.36; N, 7.36. Found: C, 51.26; H, 6.56; N, 6.48.

4.13. X-ray crystallography

CIF files representing the X-ray crystal structures of **2**, **6**, **7**, **9**, and **10** have been submitted to the Cambridge Crystallographic Database as submission numbers 767534–767538. Crystallographic data and parameters are listed below:

- $(C_5Me_5)_2U[N(SiMe_3)_2](Cl)$ (**2**): $C_{26}H_{48}ClNSi_2U$, triclinic, P-1, lattice constants $a = 8.574(2)$, $b = 9.585(2)$, $c = 18.103(4)$, $\alpha = 97.632(2)$, $\beta = 92.113(3)$, $\gamma = 104.352(2)$, $V = 1424.9(6)$ Å^3, $Z = 2$, μ(Mo-K$_\alpha$) = 5.888 mm^{-1}, $\theta_{max} = 28.21$, 6473 [$R_{int} = 0.0491$] independent reflections measured, of which 5607 were considered observed with $I > 2\sigma(I)$; max. residual electron density 4.860 and −4.100 e/Å^3; 248 parameters, $R1$ ($I > 2\sigma(I)$) = 0.0762; $wR2$ (all data) = 0.1898;
- $(C_5Me_5)_2U[N(SiMe_3)_2](NCO)$ (**6**): $C_{27}H_{48}N_2OSi_2U$, hexagonal, P63/m, lattice constants $a = 17.7701(8)$, $c = 16.1546(14)$, $\gamma = 120.00$, $V = 4417.8(5)$ Å^3, $Z = 6$, μ(Mo-K$_\alpha$) = 5.613 mm^{-1}, $\theta_{max} = 25.68$, 2915 [$R_{int} = 0.0698$] independent reflections measured, of which 2578 were considered observed with $I > 2\sigma(I)$; max. residual electron density 2.283 and −1.377 e/Å^3; 193 parameters, $R1$ ($I > 2\sigma(I)$) = 0.0431; $wR2$ (all data) = 0.1099;
- $(C_5Me_5)_2U(NPh_2)(Cl)$ (**7**): $C_{35.5}H_{44}ClNU$, monoclinic, $P21/n$, lattice constants $a = 10.5907(11)$, $b = 20.993(2)$, $c = 13.7785(15)$, $\beta = 90.1140(10)$, $V = 3063.3(6)$ Å^3, $Z = 4$, μ(Mo-K$_\alpha$) = 5.410 mm^{-1}, $\theta_{max} = 27.75$, 6147 [$R_{int} = 0.0839$] independent reflections measured, of which 4050 were considered observed with $I > 2\sigma(I)$; max. residual electron density 1.004 and −0.760 e/Å^3; 326 parameters, $R1$ ($I > 2\sigma(I)$) = 0.0359; $wR2$ (all data) = 0.0946;
- $(C_5Me_5)_2U[N(Ph)(SiMe_3)](Cl)$ (**9**): $C_{29}H_{44}ClNSiU$, monoclinic, $P21/c$, lattice constants $a = 9.4785(9)$, $b = 17.1420(16)$, $c = 18.1000(17)$, $\beta = 101.6620(10)$, $V = 2880.2(5)$ Å^3, $Z = 4$, μ(Mo-K$_\alpha$) = 5.787 mm^{-1}, $\theta_{max} = 28.33$, 6851 [$R_{int} = 0.0380$] independent reflections measured, of which 5943 were considered observed with $I > 2\sigma(I)$; max. residual electron density 0.845 and −0.627 e/Å^3; 311 parameters, $R1$ ($I > 2\sigma(I)$) = 0.0216; $wR2$ (all data) = 0.0497;
- $(C_5Me_5)_2U[N(Ph)(SiMe_3)](N_3)$ (**10**): $C_{29}H_{44}N_4SiU$, monoclinic, $P21/c$, lattice constants $a = 12.500(3)$, $b = 14.823(3)$, $c = 15.590(3)$, $\beta = 93.757(3)$, $V = 2882.4(10)$ Å^3, $Z = 4$, μ(Mo-K$_\alpha$) = 5.697 mm^{-1}, $\theta_{max} = 25.32$, 5257 [$R_{int} = 0.0851$] independent reflections measured, of which 3852 were considered observed with $I > 2\sigma(I)$; max. residual electron density 1.958 and −1.159 e/Å^3; 329 parameters, $R1$ ($I > 2\sigma(I)$) = 0.0420; $wR2$ (all data) = 0.1096.

Acknowledgements

For financial support of this work, we acknowledge the LANL G.T. Seaborg Institute for Transactinium Science (postdoctoral fellowship to R.K.T.) and the Division of Chemical Sciences, Office of Basic Energy Science, Heavy Element Chemistry program.

References

[1] P.J. Fagan, J.M. Manriquez, E.A. Maatta, A.M. Seyam, T.J. Marks, J. Am. Chem. Soc. 103 (1981) 6650.
[2] J.L. Kiplinger, K.D. John, D.E. Morris, B.L. Scott, C.J. Burns, Organometallics 21 (2002) 4306.
[3] E.J. Schelter, J.M. Veauthier, C.R. Graves, K.D. John, B.L. Scott, J.D. Thompson, J.A. Pool-Davis-Tournear, D.E. Morris, J.L. Kiplinger, Chem. Eur. J. 14 (2008) 7782.
[4] S.M. Cendrowski-Guillaume, M. Ephritikhine, J. Organomet. Chem. 577 (1999) 161.
[5] R.G. Peters, B.L. Scott, C.J. Burns, Acta Crystallogr. Sect. C Cryst. Struct. Commun. C55 (1999) 1482.
[6] G. Zi, L. Jia, E.L. Werkema, M.D. Walter, J.P. Gottfriedsen, R.A. Andersen, Organometallics 24 (2005) 4251.
[7] S.W. Hall, J.C. Huffman, M.M. Miller, L.R. Avens, C.J. Burns, A.P. Sattelberger, D.S.J. Arney, A.F. England, Organometallics 12 (1993) 752.
[8] C.R. Graves, B.L. Scott, D.E. Morris, J.L. Kiplinger, Organometallics 27 (2008) 3335.
[9] C.R. Graves, E.J. Schelter, T. Cantat, B.L. Scott, J.L. Kiplinger, Organometallics 27 (2008) 5371.
[10] R.K. Thomson, C.R. Graves, B.L. Scott, J.L. Kiplinger, Eur. J. Inorg. Chem. (2009) 1451.
[11] R.K. Thomson, T. Cantat, B.L. Scott, D.E. Morris, E.R. Batista, J.L. Kiplinger, Nature Chem. (2010) In press.
[12] D.E. Morris, R.E. Da Re, K.C. Jantunen, I. Castro-Rodriguez, J.L. Kiplinger, Organometallics 23 (2004) 5142.
[13] E.J. Schelter, R. Wu, J.M. Veauthier, E.D. Bauer, C.H. Booth, R.K. Thomson, C.R. Graves, K.D. John, B.L. Scott, J.D. Thompson, D.E. Morris, J.L. Kiplinger, Inorg. Chem. 49 (2010) 1995.
[14] E.J. Schelter, R. Wu, B.L. Scott, J.D. Thompson, D.E. Morris, J.L. Kiplinger, Angew. Chem., Int. Ed. 47 (2008) 2993.
[15] C.R. Graves, A.E. Vaughn, E.J. Schelter, B.L. Scott, J.D. Thompson, D.E. Morris, J.L. Kiplinger, Inorg. Chem. 47 (2008) 11879.
[16] C.R. Graves, P. Yang, S.A. Kozimor, A.E. Vaughn, D.L. Clark, S.D. Conradson, E.J. Schelter, B.L. Scott, J.D. Thompson, P.J. Hay, D.E. Morris, J.L. Kiplinger, J. Am. Chem. Soc. 130 (2008) 5272.
[17] D.S.J. Arney, C.J. Burns, J. Am. Chem. Soc. 115 (1993) 9840.
[18] D.S.J. Arney, C.J. Burns, J. Am. Chem. Soc. 117 (1995) 9448.
[19] L.P. Spencer, R.L. Gdula, T.W. Hayton, B.L. Scott, J.M. Boncella, Chem. Commun. (2008) 4986.
[20] W.J. Evans, C.A. Traina, J.W. Ziller, J. Am. Chem. Soc. 131 (2009) 17473.
[21] J.L. Kiplinger, D.E. Morris, B.L. Scott, C.J. Burns, Organometallics 21 (2002) 3073.
[22] K.C. Jantunen, C.J. Burns, I. Castro-Rodriguez, R.E. Da Re, J.T. Golden, D.E. Morris, B.L. Scott, F.L. Taw, J.L. Kiplinger, Organometallics 23 (2004) 4682.
[23] A.E. Clark, R.L. Martin, P.J. Hay, J.C. Green, K.C. Jantunen, J.L. Kiplinger, J. Phys. Chem. A 109 (2005) 5481.
[24] R.E. Da Re, K.C. Jantunen, J.T. Golden, J.L. Kiplinger, D.E. Morris, J. Am. Chem. Soc. 127 (2005) 682.
[25] C.C. Gatto, E.S. Lang, A. Kupfer, A. Hagenbachb, U. Abram, Z. Anorg. Allg. Chem. 630 (2004) 1286.
[26] T. Cantat, C.R. Graves, K.C. Jantunen, C.J. Burns, B.L. Scott, E.J. Schelter, D.E. Morris, P.J. Hay, J.L. Kiplinger, J. Am. Chem. Soc. 130 (2008) 17537.
[27] J.L. Kiplinger, D.E. Morris, B.L. Scott, C.J. Burns, Chem. Commun. (2002) 30.
[28] P.J. Fagan, J.M. Manriquez, S.H. Vollmer, C.S. Day, V.W. Day, T.J. Marks, J. Am. Chem. Soc. 103 (1981) 2206.
[29] J.M. Manriquez, P.J. Fagan, T.J. Marks, S.H. Vollmer, C.S. Day, V.W. Day, J. Am. Chem. Soc. 101 (1979) 5075.
[30] D.R. Lide, CRC Handbook of Chemistry and Physics, 83rd edition, 2002.
[31] I. Castro-Rodriguez, H. Nakai, K. Meyer, Angew. Chem., Int. Ed. 45 (2006) 2389.
[32] M.J. Crawford, P. Mayer, H. Noeth, M. Suter, Inorg. Chem. 43 (2004) 6860.
[33] H.M. Dietrich, J.W. Ziller, R. Anwander, W.J. Evans, Organometallics 28 (2009) 1173.
[34] B.D. Stubbert, T.J. Marks, J. Am. Chem. Soc. 129 (2007) 6149.
[35] M. Silva, M.A. Antunes, M. Dias, A. Domingos, I.C. dos Santos, J. Marcalo, N. Marques, Dalton Trans. (2005) 3353.
[36] T. Straub, W. Frank, G.J. Reiss, M.S. Eisen, J. Chem. Soc. Dalton Trans. (1996) 2541.
[37] T. Straub, A. Haskel, T.G. Neyroud, M. Kapon, M. Botoshansky, M.S. Eisen, Organometallics 20 (2001) 5017.

[38] D.L. Clark, M.M. Miller, J.G. Watkin, Inorg. Chem. 32 (1993) 772.
[39] L.R. Avens, C.J. Burns, R.J. Butcher, D.L. Clark, J.C. Gordon, A.R. Schake, B.L. Scott, J.G. Watkin, B.D. Zwick, Organometallics 19 (2000) 451.
[40] W.W. Lukens Jr., S.M. Beshouri, A.L. Stuart, R.A. Andersen, Organometallics 18 (1999) 1247.
[41] W.W. Lukens Jr., S.M. Beshouri, L.L. Blosch, A.L. Stuart, R.A. Andersen, Organometallics 18 (1999) 1235.
[42] W.J. Evans, G.W. Nyce, M.A. Johnston, J.W. Ziller, J. Am. Chem. Soc. 122 (2000) 12019.
[43] C.R. Graves, J.L. Kiplinger, Chem. Commun. (2009) 3831.
[44] C.R. Graves, B.L. Scott, D.E. Morris, J.L. Kiplinger, Chem. Commun. (2009) 776.
[45] J.L. Stewart, R.A. Andersen, New J. Chem. 19 (1995) 587.
[46] E.A. Mintz, K.G. Moloy, T.J. Marks, V.W. Day, J. Am. Chem. Soc. 104 (1982) 4692.
[47] P.G. Edwards, R.A. Andersen, A. Zalkin, Organometallics 3 (1984) 293.
[48] J.L. Kiplinger, D.E. Morris, B.L. Scott, C.J. Burns, Organometallics 21 (2002) 5978.
[49] J.C. Berthet, P. Thuery, M. Ephritikhine, Eur. J. Inorg. Chem. (2008) 5455.
[50] A.B.P. Lever, Inorganic Electronic Spectroscopy, 2nd ed., Elsevier, Amsterdam, 1984.
[51] A.B.P. Lever, E.S. Dodsworth, Electrochemistry, Charge transfer spectroscopy and electronic structure, in: E.I. Solomon, A.B.P. Lever (Eds.) inorganic electronic structure and spectroscopy, John Wiley & Sons, Inc., New York, 1999, pp. 227-290.
[52] C.R. Graves, B.L. Scott, D.E. Morris, J.L. Kiplinger, J. Am. Chem. Soc. 129 (2007) 11914.
[53] Bruker-AXS, SAINT 7.06, Integration Software, Bruker Analytical X-ray Systems, Madison, WI, 2003.
[54] G.M. Sheldrick, SHELXTL 5.10, Structure Solution and Refinement Package, University of Göttingen, Göttingen, Germany, 1997.
[55] G.M. Sheldrick, SADABS 2.03, Program for Adsorption Correction, University of Göttingen, Göttingen, Germany, 2001.
[56] R.K. Thomson, C.R. Graves, B.L. Scott, J.L. Kiplinger, Dalton Trans., (2010) In press.
[57] N. Camire, U.T. Mueller-Westerhoff, W.E. Geiger, J. Organomet. Chem. 637–639 (2001) 823.
[58] R.J. LeSuer, W.E. Geiger, Angew. Chem., Int. Ed. 39 (2000) 248.
[59] R.J. LeSuer, C. Buttolph, W.E. Geiger, Anal. Chem. 76 (2004) 6395.